[2.2]Paracyclophane-Bridged Mixed-Valence Compounds: Application of a Generalized Mulliken−Hush Three-Level Model

Stephan Amthor and Christoph Lambert*

Institut für Organische Chemie, Universität Würzburg, Am Hubland, D-97074 Würzburg, Germany

Received: September 6, 2005; In Final Form: October 28, 2005

A series of [2.2]paracylophane-bridged bis-triarylamine mixed-valence (MV) radical cations were analyzed by a generalized Mulliken−Hush (GMH) three-level model which takes two transitions into account: the intervalence charge transfer (IV-CT) band which is assigned to an optically induced hole transfer (HT) from one triarylamine unit to the second one and a second band associated with a triarylamine radical cation to bridge (in particular, the [2.2]paracyclophane bridge) hole transfer. From the GMH analysis, we conclude that the [2.2]paracyclophane moiety is not the limiting factor which governs the intramolecular charge transfer. AM1-CISD calculations reveal that both through-bond as well as through-space interactions of the [2.2]-paracyclophane bridge play an important role for hole transfer processes. These electronic interactions are of course smaller than direct π-conjugation, but from the order of magnitude of the couplings of the [2.2]-paracyclophane MV species, we assume that this bridge is able to mediate significant through-space and through-bond interactions and that the cyclophane bridge acts more like an unsaturated spacer rather than a saturated one. From the exponential dependence of the electronic coupling V between the two triarylamine localized states on the distance r between the two redox centers, we infer that the hole transfer occurs via a superexchange mechanism. Our analysis reveals that even significantly longer π-conjugated bridges should still mediate significant electronic interactions because the decay constant β of a series of π-conjugated MV species is small.

Introduction

Both intermolecular and intramolecular charge transfer in π-conjugated molecules are of fundamental interest for the development of conducting and semiconducting materials for organic electronic devices. While charge transfer along conjugated backbones is usually quite fast, it is the charge transfer between the conjugated systems that limits the overall charge transfer rate. In the present study, we present the synthesis and investigate the optically induced hole transfer processes of model systems in which the π-faces of two triarylamine moieties are brought in close contact by a [2.2]paracyclophane unit.

The [2.2]paracyclophane moiety is a simple scaffold to bring chromophores in close contact even beyond the van der Waals distance in order to examine interactions based on through-bond (σ) and through-space ($\pi-\pi$) couplings without having direct π-conjugation.[1−10] It has been demonstrated by Heilbronner and Maier that both couplings, through-bond (σ) and through-space, are of importance for electronic interactions in [2.2]paracyclophanes.[11] In this context, the investigation of charged cyclophane systems is of great interest for studying charge-transfer processes over the [2.2]paracyclophane moiety. While the oxidation of unsubtituted [2.2]paracyclophane to the corresponding radical cation is irreversible in solution,[12] the radical anion of [2.2]-paracyclophane is more persistent.[13−16] Badger and Brocklehurst reported absorption spectra of both the radical anion and the radical cation of [2.2]paracyclophane which were generated by γ-radiolysis of glassy solutions at low temperatures.[17] The absorption spectrum of the radical cation was compared with the photoelectron spectrum of neutral [2.2]paracylophane by Heilbronner et al.[18] By ESR and ENDOR spectroscopy it was shown that a substitution of [2.2]paracyclophane by electron donating groups such as methyl or methoxy substituents leads to a stabilization of the corresponding radical cations.[16,19−22] By these methods, a strong intramolecular electronic coupling between the two aromatic subunits was found which is in agreement with the interpretation of the absorption signal of the [2.2]paracyclophane radical cation as a charge resonance band by Badger and Brocklehurst.[17] The Mulliken−Hush theory was recently applied to the absorption spectra of dinitro-[2.2]-paracyclophane radical anions.[23] In this study, the authors found that the pseudo-para isomer is a class III mixed-valence system where the charge is completely delocalized over the hole cyclophane while the pseudo-ortho isomer is supposed to be at the class II/class III borderline where, depending on the solvent polarity, the charge is either localized (class II) on one molecular half or delocalized (class III).

Triarylamine moieties have recently been used as redox centers in a number of mixed-valence (MV) compounds[24−51] and redox cascades[52] in order to study hole transfer processes. MV species are generally characterized by at least two redox centers with unequal formal oxidation states. In the study presented here, we use the cyclophane moiety as the bridging unit between two triarylamine redox centers (see Chart 1; for synthetic details, see Supporting Information). In the resulting MV radical ions $[N-B-N]^+$, the distance between the two charge bearing units N was varied from $\mathbf{1}^{\bullet+}$ over $\mathbf{4}^{\bullet+}$ to $\mathbf{9}^{\bullet+}$. The two isomers pseudo-para [2.2]paracyclophane $\mathbf{4}^{\bullet+}$ and pseudo-ortho isomer $\mathbf{5}^{\bullet+}$ were used to investigate the influence of the connectivity on hole transfer (HT) processes. For the comparison of the through-bond and through-space interactions

* To whom correspondence should be addressed. E-mail: lambert@chemie.uni-wuerzburg.de.

10.1021/jp0550309 CCC: $33.50
Published on Web 12/21/2005

CHART 1

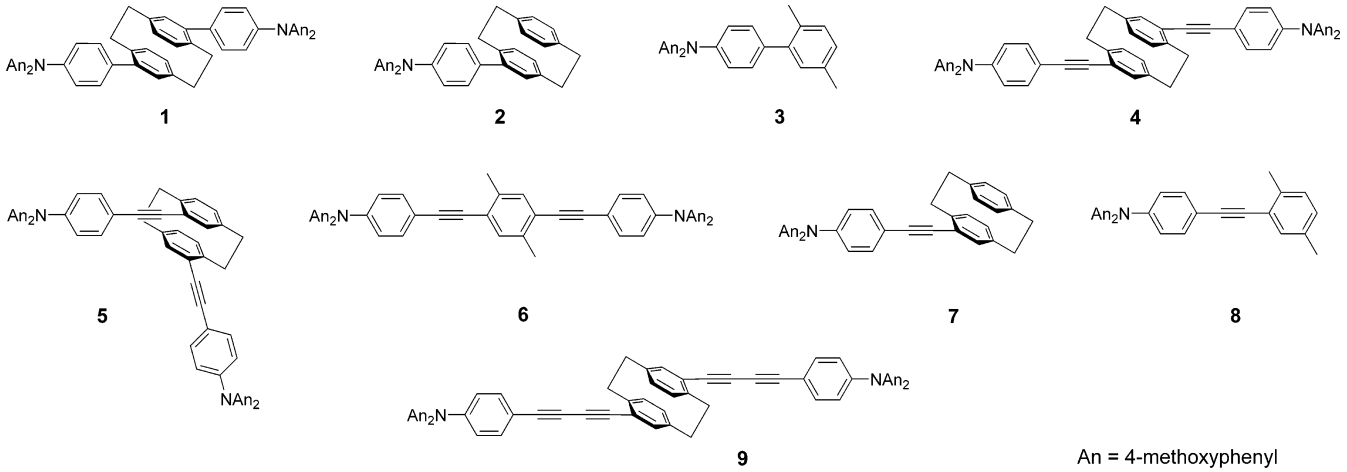

of the [2.2]paracyclophane bridge with direct π-conjugation, the *p*-xylene bridge was used in compound $\mathbf{6}^{\bullet+}$. The vis/near-infrared (NIR) spectra of the MV compounds were analyzed by a generalized Mulliken−Hush (GMH)[53−55] three-level model using both experimental transition energies and transition moments as well as AM1-CISD computed values in order to calculate the diabatic electronic coupling matrix elements which yield information about the electronic interactions of the MV species.

In the three-level GMH model, which we have recently applied for similar MV compounds,[34,44] two transitions are taken into account: on one hand, the intervalence charge transfer (IV-CT) band which is assigned to an optically induced hole transfer from one redox center to the second and, on the other hand, a second band associated with a triarylamine radical cation to bridge hole transfer, hereafter called the "bridge band". Therefore, three levels have to be used for a proper description of the MV properties: the ground state (g), the first excited IV-CT state (a), and the second excited bridge state (b) (see Figure 1).

Taking the bridge band into account is particularly necessary if the MV species show an intense bridge band and the dipole moment difference between the ground (g) and the first excited (a) IV-CT state is relatively small.[44] In this paper, the results of the GMH analysis of the MV compounds will be used to evaluate the potential energy surfaces (PESs) of the three states within a semiclassical two-mode model.

Results and Discussion

Evaluation of Diabatic Electronic Couplings (*V*) by GMH Theory. GMH theory developed by Newton and Cave[54] can be applied for the description of charge-transfer excitations in a system with any number of excited states *n* and has often been used within a two-level model for the analysis of IV-CT absorption properties from experimental or computational data.[56−62] Within the two-level approach, the GMH is equivalent to the well-known Mulliken−Hush formalism (eq 1) with the experimental transition moment μ_{ga} (see eq 2) and the transition energy $\tilde{\nu}_a$ and the diabatic dipole moment difference $\Delta\mu_{12}$. The

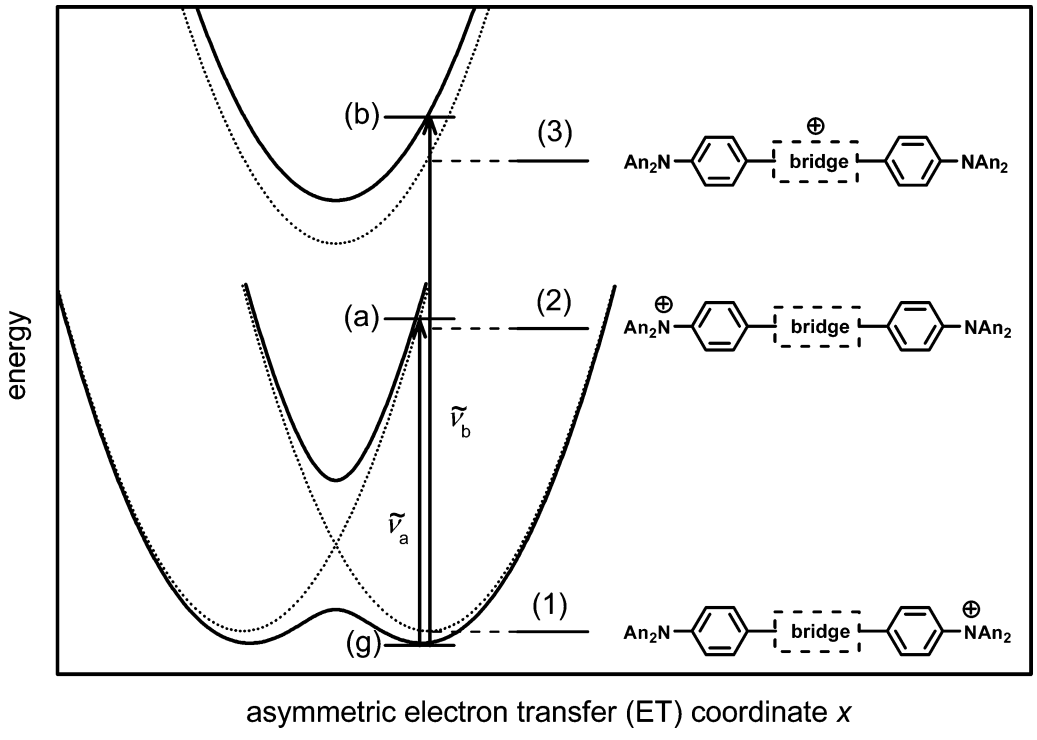

Figure 1. Adiabatic (black solid) and diabatic (dotted) states within a GMH three-level model.

latter quantity can be traced back to purely adiabatic quantities (eq 3), where μ_{gg} and μ_{aa} are the dipole moments of the ground and the excited IV-CT states, respectively.

$$V_{\text{two-level}} = \frac{\mu_{ga}\tilde{\nu}_a}{\Delta\mu_{12}} \quad (1)$$

$$\mu_{ga} = 0.09584\sqrt{\frac{\int \epsilon(\tilde{\nu})\, d\tilde{\nu}}{\tilde{\nu}_a}} \quad (2)$$

$$\Delta\mu_{12} = \mu_{22} - \mu_{11} = \sqrt{(\mu_{aa} - \mu_{gg})^2 + 4\mu_{ga}{}^2} \quad (3)$$

In this paper, we use a three-level model which takes into account the ground state (g), the IV-CT state (a), and the bridge state (b). The transition moments and dipole moments of these states yield the adiabatic matrix μ_{adiab} (eq 4).[63] The transition moments for the IV-CT excitation (μ_{ga}) and the bridge excitation (μ_{gb}) can both be obtained by band integration of the experimental spectrum (eq 2). In contrast, the transition moment μ_{ab} between these excited states (a) and (b) as well as the dipole moments μ_{gg}, μ_{bb}, and μ_{aa} of the three levels (g), (a), and (b) are difficult to evaluate experimentally, and, therefore, are calculated by quantum chemical methods in the present study.

$$\mu_{adiab} = \begin{pmatrix} \mu_{gg} & \mu_{ga} & \mu_{gb} \\ \mu_{ga} & \mu_{aa} & \mu_{ab} \\ \mu_{gb} & \mu_{ab} & \mu_{bb} \end{pmatrix} \quad (4)$$

$$\mu_{diab} = \begin{pmatrix} \mu_{11} & 0 & 0 \\ 0 & \mu_{22} & 0 \\ 0 & 0 & \mu_{33} \end{pmatrix} \quad (5)$$

The GMH theory defines diabatic (model) levels which are strictly localized and, therefore, have vanishing transition dipole moments between all states. Thus, all off-diagonal elements of the diabatic transition moment matrix μ_{diab} (eq 5) are zero. Within this assumption, the GMH theory uses a unitary transformation of the adiabatic transition moment matrix into the corresponding diabatic matrix according to $\mu_{diab} = \mathbf{C}^t\mu_{adiab}\mathbf{C}$. This is done by applying the diagonalization matrix **C** which consists of the normalized eigenvectors of μ_{adiab}. The same unitary transformation with an identical matrix **C** is then applied to the adiabatic energy matrix $\mathbf{H}_{diab} = \mathbf{C}^t\mathrm{H}_{adiab}\mathbf{C}$. The adiabatic energy matrix (eq 6) consists of adiabatic energy differences between the ground state (g) and the first excited state (a) as well as the ground state (g) and the second excited state (b). These values are measurable quantities since they correspond to the transition energies of the IV-CT band ($\tilde{\nu}_a$) and the bridge band ($\tilde{\nu}_b$).

$$\mathbf{H}_{adiab} = \begin{pmatrix} 0 & 0 & 0 \\ 0 & \tilde{\nu}_a & 0 \\ 0 & 0 & \tilde{\nu}_b \end{pmatrix} \quad (6)$$

The resulting diabatic energy matrix (eq 7) then contains the energies of the diabatic states (1−3) as the diagonal elements H_{11}, H_{22}, and H_{33} and, in addition, the electronic couplings V_{12}, V_{13}, and V_{23} between these states as the off-diagonal elements.

$$\mathbf{H}_{diab} = \begin{pmatrix} H_{11} & V_{12} & V_{13} \\ V_{12} & H_{22} & V_{23} \\ V_{13} & V_{23} & H_{33} \end{pmatrix} \quad (7)$$

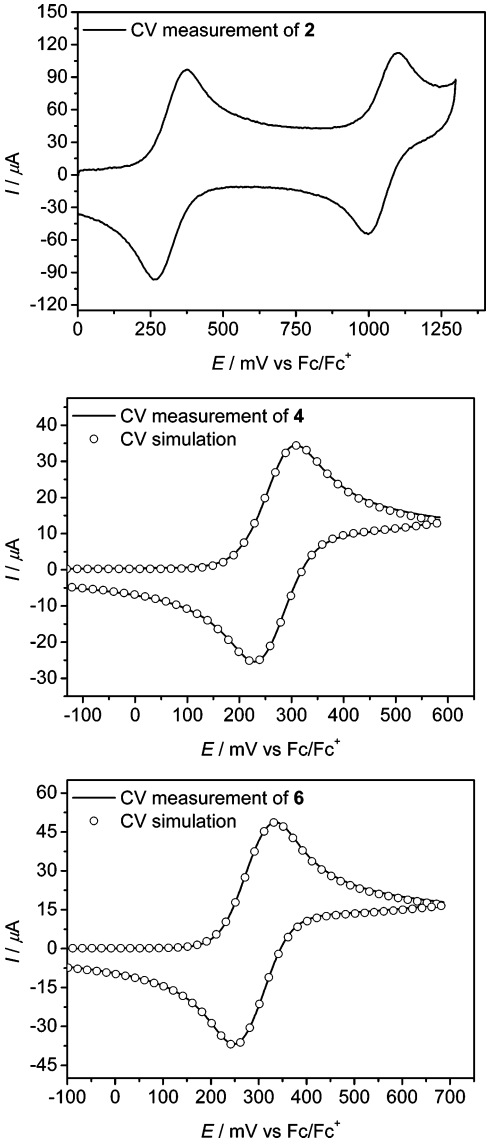

Figure 2. Cyclic voltammograms of **2** (v = 5000 mV s^{-1}), **4**, and **6** (both v = 250 mV s^{-1}) in CH_2Cl_2/0.15 TBAH and digital simulations of the CVs of **4** and **6**.

These couplings are a measure for the electronic interactions between the diabatic states and, therefore, important for the description of the optoelectronic properties of MV systems. At this point, we mention that the couplings V in general depend on the nuclear motion but are evaluated here using the Condon approximation.

Electrochemical Properties. All compounds **1**−**9** show a first oxidation wave between 200 and 300 mV vs ferrocene/ferrocenium (Fc/Fc^+) as the internal standard in CH_2Cl_2/0.15 M tetrabutylammonium hexafluorophosphate (TBAH). This first oxidation wave is reversible for all molecules even under thin layer conditions and is associated with a one-electron oxidation of the nitrogen center of mono-triarylamines and with a sequence of two one-electron oxidations of the first and the second nitrogen center of the bis-triarylamines.

As the peak separation is invisibly small for all bis-triarylamines, digital simulations of the voltammograms were used in order to determine the absolute values of the two redox potentials (see Figure 2 and Table 1). The first oxidation potential of biaryl compounds **1**−**3** is within a 200−225 mV range while molecules containing an acetylene spacer show higher

TABLE 1: Redox Potentials of 1−9[a] Measured by Cyclic Voltammetry in CH_2Cl_2/0.15 TBAH vs Fc/Fc^+

	$E_{1/2}(I)^b$/mV	$E_{1/2}(II)^b$/mV	ΔE^c		$E_{1/2}(I)^b$/mV	$E_{1/2}(II)^b$/mV	ΔE^c
1	200	250	50	**6**	270	320	50
2	205	925		**7**	265	1000[d]	
3	225			**8**	270		
4	240	290	50	**9**	290	340	50
5	250	300	50				

[a] The redox potentials of **1**, **4**, **5**, **6**, and **9** were determined by digital simulation of the voltammograms. [b] ±3 mV. [c] ±4 mV. [d] Peak potential of an irreversible oxidation process.

redox potentials between 240 and 270 mV and **9** with two butadiyne spacers shows the highest redox potential at 290 mV.

The potential splittings between the first and the second oxidation are small due to the large distance between the two triarylamine redox centers in **1**, **4**, **5**, **6**, and **9**. The absolute ΔE values of all bis-triarylamines are similar within the experimental error. The fact that all ΔE values are somewhat larger than the statistical value of 35.6 mV for noninteracting redox centers is a hint that the two redox centers in MV species interact weakly. Thus, the monoradical cations $\mathbf{1}^{\bullet+}$, $\mathbf{4}^{\bullet+}$, $\mathbf{5}^{\bullet+}$, $\mathbf{6}^{\bullet+}$, and $\mathbf{9}^{\bullet+}$ are expected to be IV-CT systems of Robin−Day class II. For mono-triarylamine **2**, a second oxidation wave at 925 mV which is reversible only at high scan rates ($\upsilon = 5000$ mV s^{-1}) was observed as well as a third irreversible oxidation at $E_p(III) = 1305$ mV. For compound **7**, there is a second oxidation peak at 1000 mV which proved to be irreversible. The second oxidation wave of **2** and **7** is associated with a second one-electron oxidation of the nitrogen center, while the third oxidation wave of **2** is interpreted as an irreversible oxidation of the paracyclophane moiety.

Experimental Vis/NIR Spectra. The absorption spectra of the MV species $\mathbf{1}^{\bullet+}$, $\mathbf{4}^{\bullet+}$, $\mathbf{5}^{\bullet+}$, $\mathbf{6}^{\bullet+}$, and $\mathbf{9}^{\bullet+}$ in CH_2Cl_2 and in MeCN (except $\mathbf{9}^{\bullet+}$) were obtained by stepwise chemical oxidation of the corresponding neutral compounds and are shown in Figure 3. For comparison, the spectra of the mono-triarylamine radical cations $\mathbf{2}^{\bullet+}$, $\mathbf{3}^{\bullet+}$, $\mathbf{7}^{\bullet+}$, and $\mathbf{8}^{\bullet+}$ in CH_2Cl_2 obtained in an analogous manner are also presented.

All MV species show a typical absorption band in the NIR region between 6230 and 7500 cm^{-1} which is associated with an optically induced intramolecular hole transfer from the oxidized triarylamine moiety to the second neutral triaryalmine unit. This IV-CT absorption shows a distinct blue shift in MeCN compared to the less polar CH_2Cl_2. This solvatochromism proves the pronounced CT character of the transition and can be explained by an increase of solvent reorganization energy in MeCN vs CH_2Cl_2. Accordingly, in the vis/NIR spectra of the mono-triarylamine radical cations, no absorption signals in the NIR region are found as no intramolecular charge transfer can occur. The second absorption band of the MV compounds lies between 10 680 and 11 870 cm^{-1} and is assigned to a hole transfer from the oxidized triarylamine moiety to the bridging unit. This bridge band also appears in the spectra of the mono-triarylamine radical cations $\mathbf{2}^{\bullet+}$, $\mathbf{3}^{\bullet+}$, $\mathbf{7}^{\bullet+}$, and $\mathbf{8}^{\bullet+}$. It is obvious that compounds with identical spacers and "bridging" units as, for example, $\mathbf{1}^{\bullet+}$ and $\mathbf{2}^{\bullet+}$ have nearly identical transition energies $\tilde{\nu}_b$ in CH_2Cl_2. The bridge band of all MV species also shows a distinct blue shift in MeCN which is again explained by an increase in the solvent reorganization energy. In addition to the IV-CT and the bridge band, all MV species as well as the mono-triarylamine radical cations exhibit an additional band between 13 000 and 13 500 cm^{-1} which lacks any pronounced solvatochromism. This so-called $\pi-\pi^*$ band is typical of triarylamine radical cations $\mathbf{1}^{\bullet+}-\mathbf{9}^{\bullet+}$. It can be assigned to a dianisylamine localized charge resonance transition.[64] For a more detailed analysis of the absorption bands of the MV compounds, we deconvoluted the spectra in CH_2Cl_2 by four (five for $\mathbf{1}^{\bullet+}$) Gaussian functions. A single Gaussian function was fitted to the IV-CT band, and this function was used for the calculation of the transition moment μ_{ga} according to eq 2 for all MV compounds. Because the IV-CT band of $\mathbf{1}^{\bullet+}$ is slightly asymmetric, an additional function was fitted to the high-energy side of this band. The bridge band was fitted in a similar way by a second single Gaussian function which was used to obtain the transition energy $\tilde{\nu}_b$ as well as the transition moment μ_{gb} (see Table 2). Two further Gaussian functions were combined to fit the $\pi-\pi^*$ band of the spectra. The strong overlap of the absorption signals in MeCN precludes deconvolution by Gaussian functions and made a GMH analysis of the MV systems in the more polar solvent MeCN impossible.

The vis/NIR absorption spectra of the mono-triarylamines $\mathbf{2}^{\bullet+}$, $\mathbf{7}^{\bullet+}$, and $\mathbf{8}^{\bullet+}$ were fitted by three Gaussian functions. A single function was fitted to the bridge band, and two Gaussian functions were fitted to the $\pi-\pi^*$ absorption signal. For the radical cation $\mathbf{3}^{\bullet+}$, two functions were fitted to each absorption signal.

The extinction coefficient ϵ and, thus, the transition moment μ_{ga} of the MV compound with the largest N−N distance $\mathbf{9}^{\bullet+}$ are much smaller than those of the three paracyclophane bridged MV compounds $\mathbf{1}^{\bullet+}$, $\mathbf{4}^{\bullet+}$, and $\mathbf{5}^{\bullet+}$. The [2.2]paracyclophane $\mathbf{1}^{\bullet+}$ and the π-conjugated *p*-xylene $\mathbf{6}^{\bullet+}$ show the most intense IV-CT band with the largest transition moments μ_{ga}. We therefore expect the strongest electronic interactions in $\mathbf{6}^{\bullet+}$ and $\mathbf{1}^{\bullet+}$ and the weakest interactions in $\mathbf{9}^{\bullet+}$. The bridge band transition moments μ_{gb} of all bis-triarylamines $\mathbf{1}^{\bullet+}$, $\mathbf{4}^{\bullet+}-\mathbf{6}^{\bullet+}$, and $\mathbf{9}^{\bullet+}$ are very similar.

In a recent study, we found empirically a linear relationship between the oscillator strength and the absorption energy $\tilde{\nu}$ of a series of triarylamine radical cations.[64] We therefore calculated the oscillator strengths f_{gb} of the MV species and mono-triarylamines $\mathbf{2}^{\bullet+}$, $\mathbf{7}^{\bullet+}$, and $\mathbf{8}^{\bullet+}$ by eq 8 and plotted the resulting f_{gb} values vs the absorption energy $\tilde{\nu}_b$ (see Figure 4).

$$f_{gb} = \frac{4.7014 \times 10^{-7} \tilde{\nu}_b \mu_{gb}^{\ 2}}{\mathrm{cm}^{-1}\,\mathrm{D}^2} \qquad (8)$$

Compound $\mathbf{3}^{\bullet+}$ was neglected as it is difficult to determine the energy $\tilde{\nu}_b$ as well as the oscillator strength exactly due to strong overlap of the absorption bands (see Figure 3). Figure 4 clearly demonstrates that the oscillator strength of the bridge band f_{gb} decreases approximately linearly with increasing transition energy $\tilde{\nu}_b$. As the bridge band of $\mathbf{5}^{\bullet+}$ has the smallest absorption energy $\tilde{\nu}_b$, compound $\mathbf{5}^{\bullet+}$ has the highest oscillator strength f_{gb} and, consequently, the smallest transition moment μ_{ga}. As can be seen in Figure 4, the cyclophane $\mathbf{1}^{\bullet+}$ is an exception because it does not fulfill the correlation of f_{gb} and $\tilde{\nu}_b$.

At present, we have no quantitative description nor a physical interpretation for the linear correlation of f_{gb} and $\tilde{\nu}_b$. Nevertheless, our finding is in accordance with that of our recent study of a series of triarylamine radical cations[64] and also in agreement with a study of Zhu and Wolf[66] who obtained a linear relationship between the oscillator strength *f* and the transition energy $\tilde{\nu}$ for (ferrocenylethynyl)oligothiophene complexes as well.

AM1-CISD Computations and Evaluation of Electronic Couplings by GMH Theory. In a recent work, we used the GMH three-level model for a general analysis of electronic

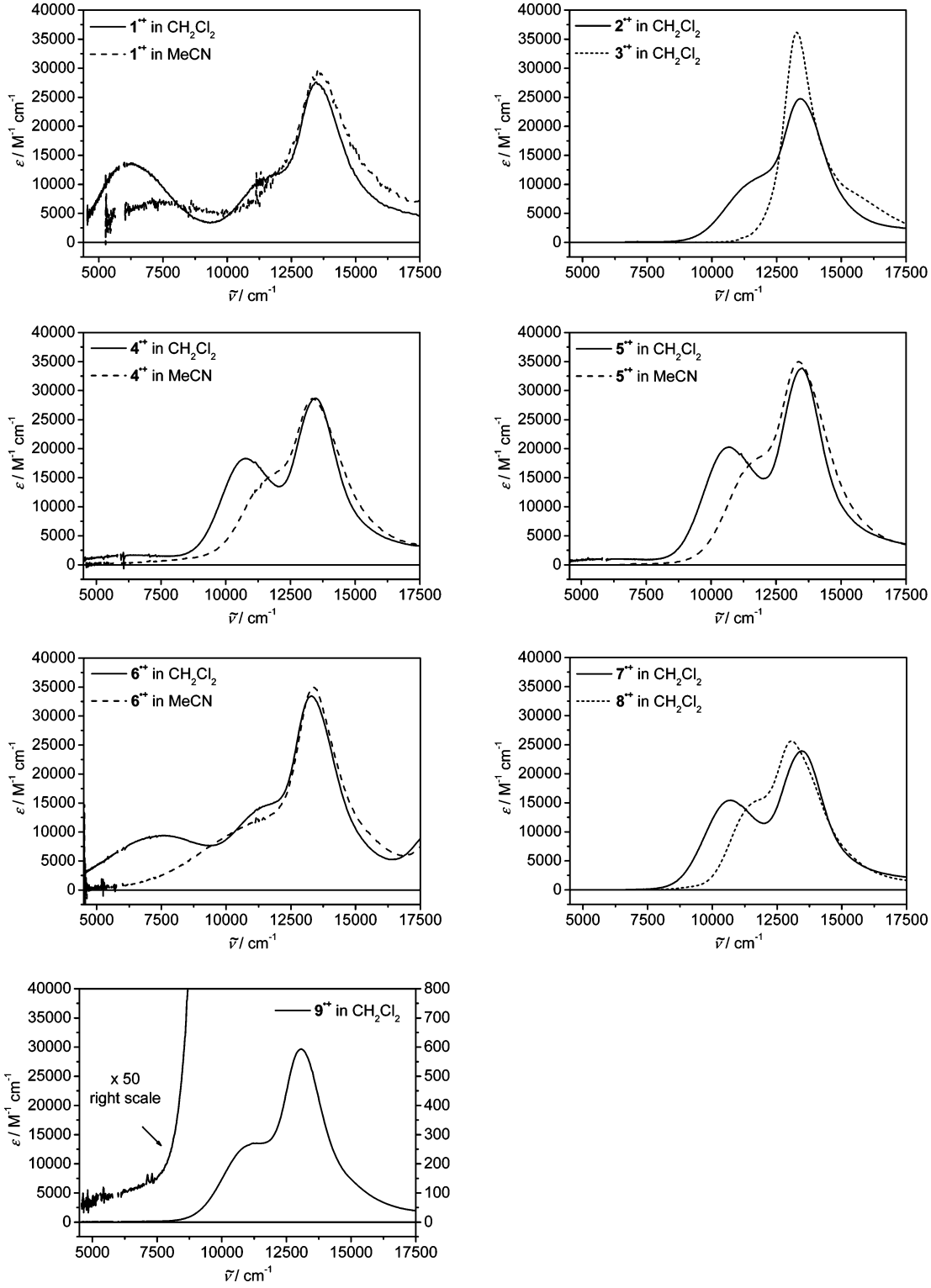

Figure 3. Experimental absorption spectra of mixed-valence species $\mathbf{1}^{\bullet+}$, $\mathbf{4}^{\bullet+}$, $\mathbf{5}^{\bullet+}$, $\mathbf{6}^{\bullet+}$, and $\mathbf{9}^{\bullet+}$ in CH_2Cl_2 and in MeCN (except $\mathbf{9}^{\bullet+}$) and spectra of mono-triarylamine radical cations $\mathbf{2}^{\bullet+}$, $\mathbf{3}^{\bullet+}$, $\mathbf{7}^{\bullet+}$, and $\mathbf{8}^{\bullet+}$ in CH_2Cl_2.

couplings depending on the transition moments and the relative transition energies of IV-CT and bridge bands.[44] We were able to demonstrate that the three-level model is necessary for a more precise description of MV systems if they show an intense bridge band and if the dipole moment difference between the ground μ_{gg} and the first excited IV-CT state μ_{aa} are relatively small. To examine the dependence of the couplings on the relative energy of the bridge state $\tilde{\nu}_b$, we used a given set of parameters (see Figure 5) and the following simplified adiabatic transition moment matrix (eq 9) as input for a GMH analysis. In this matrix, the dipole moment μ_{gg} is subtracted from the diagonal elements and, as a reasonable approximation, the difference $\mu_{bb} - \mu_{gg}$ was set to $(\mu_{aa} - \mu_{gg})/2$. The set of parameters used applies to a strongly localized MV compound.

$$\mu_{adiab} = \begin{pmatrix} 0 & \mu_{ga} & \mu_{gb} \\ \mu_{ga} & \Delta\mu_{ag} = \mu_{aa} - \mu_{gg} & \mu_{ab} \\ \mu_{gb} & \mu_{ab} & \Delta\mu_{ag}/2 \end{pmatrix} \qquad (9)$$

As shown in Figure 5a, the couplings calculated by the three-

TABLE 2: Experimental Data Obtained from vis/NIR Spectra Recorded in CH_2Cl_2 and Spectra Deconvolution by Gaussian Functions

	$\tilde{\nu}_a$[a]/cm^{-1}	$\Delta\tilde{\nu}_{1/2}$[b]/cm^{-1}	ϵ[c]/cm^{-1}	μ_{ga}/D	$\tilde{\nu}_b$[a]/cm^{-1}	$\Delta\tilde{\nu}_{1/2}$[b]/cm^{-1}	ϵ[c]/cm^{-1}	μ_{gb}/D	$\tilde{\nu}_{\pi-\pi^*}$[a]/cm^{-1}	ϵ[c]/cm^{-1}
1$^{\bullet+}$[d]	6230	2700	13 900	7.6 ± 0.3	11 870 (sh)	3240	11 700	5.4 ± 0.3	13 480	27 800
2$^{\bullet+}$					11 500	2490	10 500	4.6 ± 0.3	13 400	24 700
3$^{\bullet+}$					15 500 (sh)	2840	8600	3.9 ± 0.2	13 260	36 200
4$^{\bullet+}$	6600	4570	1700	3.4 ± 0.1	10 700	2120	18 300	5.9 ± 0.3	13 480	28 700
5$^{\bullet+}$	6280	4340	1000	2.6 ± 0.1	10 680	2150	20 300	6.3 ± 0.3	13 510	33 900
6$^{\bullet+}$	7500	4660	9400	7.6 ± 0.3	11 590 (sh)	2580	14 600	5.3 ± 0.3	13 300	33 400
7$^{\bullet+}$					10 680	2180	15 400	5.3 ± 0.3	13 440	23 900
8$^{\bullet+}$					11 500 (sh)	1670	14 900	4.1 ± 0.2	13 050	25 600
9$^{\bullet+}$	7500	4890	150	0.9 ± 0.03	11 100	2350	13 400	5.2 ± 0.3	13 050	29 700

[a] ±200 cm^{-1}. [b] bandwidth at half-height ±200 cm^{-1}. [c] ±5%. [d] Estimated under the assumption that the monoradical cation **1**$^{\bullet+}$ shows a $\pi-\pi^*$ band half as intense as the dication **1**$^{2+}$.[65]

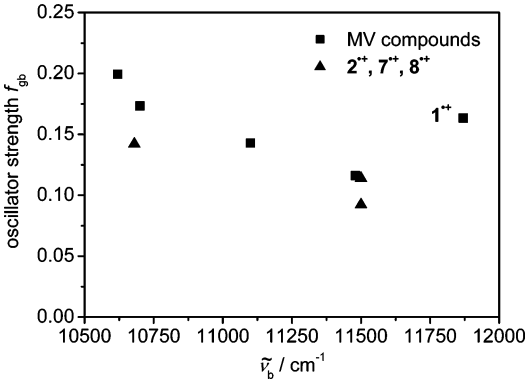

Figure 4. Plot of the oscillator strength f_{gb} of the bridge band vs the corresponding absorption energy of the MV compounds (■) and mono cations **2**$^{\bullet+}$, **7**$^{\bullet+}$, and **8**$^{\bullet+}$ (▲).

level model reveal a linear correlation to $\tilde{\nu}_b$ if the transition moment for the bridge state μ_{gb} is kept constant. Therefore, the deviation of V_{12} from $V_{two-state}$ (eq 1) increases with the increasing energy of the bridge state $\tilde{\nu}_b$.[44] However, a more realistic set of parameters should also consider the empirically found correlation between μ_{gb} and $\tilde{\nu}_b$ (Figure 4). Thus, because $\mu_{gb} \sim (f_{gb})^{1/2}/\tilde{\nu}_b$, we implied the relation $\mu_{gb} = (25 - 5\tilde{\nu}_b)^{1/2}/\tilde{\nu}_b$ in our general GMH analysis which is shown in Figure 5b. The given empirical relation for μ_{gb} was chosen so that μ_{gb} has a realistic value (4.5) for $\tilde{\nu}_b = 1$ and that μ_{gb} becomes zero for the limit of the plot $\tilde{\nu}_b = 5$.

In this more sophisticated representation, only the coupling V_{23} shows a linear correlation at $\tilde{\nu}_b > 1$ while V_{12} is very similar to $V_{two-state}$ even at high $\tilde{\nu}_b$ energy values due to the fact that the transition moment μ_{gb} approaches zero. Thus, for strongly localized MV systems, V_{12} depends only weakly on the energy of the bridge state $\tilde{\nu}_b$ while V_{13} and V_{23} show a more pronounced dependence on $\tilde{\nu}_b$.We suppose that including the relationship between μ_{gb} and $\tilde{\nu}_b$ gives a more realistic model to predict the behavior of coupling values as a function of the energy of the bridge state.

To analyze the MV compounds **1**$^{\bullet+}$, **4**$^{\bullet+}$−**6**$^{\bullet+}$, and **9**$^{\bullet+}$ by the GMH three-level model data for μ_{gg} and μ_{aa}, μ_{bb} and μ_{ab} are required in addition to our experimental values for $\tilde{\nu}_a$, $\tilde{\nu}_b$, μ_{ga}, and μ_{gb}. We have previously demonstrated that AM1-CISD computations may be used for the evaluation of these four missing data and that the results are physically reasonable.[44] Thus, we optimized the ground-state geometry at the AM1-CISD level with an active orbital window consisting of four doubly occupied orbitals, one singly occupied orbital, and two unoccupied orbitals. To calculate the transition moments and dipole moments, we used the gas-phase optimized ground-state structures and calculated single SCF cycles at the AM1-CISD level. For the simulation of a solvent environment with ϵ = 2.0, we used the conductor-like screening model (COSMO) and calculated single points at the gas-phase optimized structures in the same way. The computational results are collected in Table 3 and in Table 4. The adiabatic transition moments derived from AM1-CISD calculation in the gas phase and with the COSMO solvent model and the experimental values (exp.) are given in Table 3 where the diagonal elements of the diabatic transition moment matrix μ_{diab} (eq 5) derived from the GMH three-level model are also presented. All given transition dipole moments are the projections of the respective vectors on the vector connecting the two nitrogen redox centers.

The computed and experimental adiabatic transition energy values and the electronic couplings V (off-diagonal elements of the diabatic energy matrix $\mathbf{H}_{diab}$ (eq 7)) derived from the GMH three-level model and, in addition, the couplings $V_{two-level}$ of the GMH two-level model estimated by eq 1 are given in Table 4. We used the AM1-CISD + COSMO computed values for μ_{gg}, μ_{aa}, μ_{bb}, and μ_{ab} to complete the given experimental values for the GMH three-level analysis.

Because absolute dipole moments of ions are origin dependent,[63] we rest the discussion in the following on dipole moment differences projected on the N−N axis of the molecules (see Table 5). The dipole moment differences $\Delta\mu_{ag} = \mu_{aa} - \mu_{gg}$ in a solvent with $\epsilon = 2.0$ for all MV compounds is between 42.4 D (**5**$^{\bullet+}$) and 98.7 D (**9**$^{\bullet+}$). The dipole moment differences $\Delta\mu_{bg} = \mu_{bb} - \mu_{gg}$ are roughly half of $\Delta\mu_{ag}$ (e.g., 20.1 D for **5**$^{\bullet+}$ and 52.1 D for **9**$^{\bullet+}$). Thus, the corresponding states can easily be identified as the bridge state and the IV-CT state, respectively. From the values above, it is clear that the assumption made in Figure 5 to set $\Delta\mu_{bg} = \Delta\mu_{ag}/2$ is quite reasonable. Deviations from this relation are due to invalidity of the Condon approximation. As expected, the diabatic dipole moment differences $\Delta\mu_{12} = \mu_{22} - \mu_{11}$ and $\Delta\mu_{13} = \mu_{33} - \mu_{11}$ are all somewhat larger than the corresponding adiabatic values. The diabatic differences $\Delta\mu_{12}$ correspond to unit charge-transfer distances of 14.1 Å for **1**$^{\bullet+}$, 9.0 Å for **5**$^{\bullet+}$, and 21.1 Å for **9**$^{\bullet+}$ which are somewhat smaller than the geometric N−N distances (15.1 Å **1**$^{\bullet+}$, 9.9 Å **5**$^{\bullet+}$, and 25.0 Å **9**$^{\bullet+}$). The corresponding diabatic unit charge transfer distances are even distinctly smaller in the MV compounds **4**$^{\bullet+}$ (14.4 Å, N−N = 19.9 Å) and **6**$^{\bullet+}$ (11.7 Å, N−N = 19.3 Å). This behavior reflects stronger charge delocalization into the bridge in the latter cases, in particular in the π-conjugated system **6**$^{\bullet+}$.

The gas-phase computed transition moments μ_{ga} and μ_{gb} are in bad agreement with the experimental transition moments. In general, transition moments are difficult to calculate even at a much higher level of theory. However, including the COSMO solvent model in our computation yields transition moments which are in significantly better agreement for all compounds with the exception of *p*-xylene **6**$^{\bullet+}$. The fact that μ_{ga} and μ_{ab}

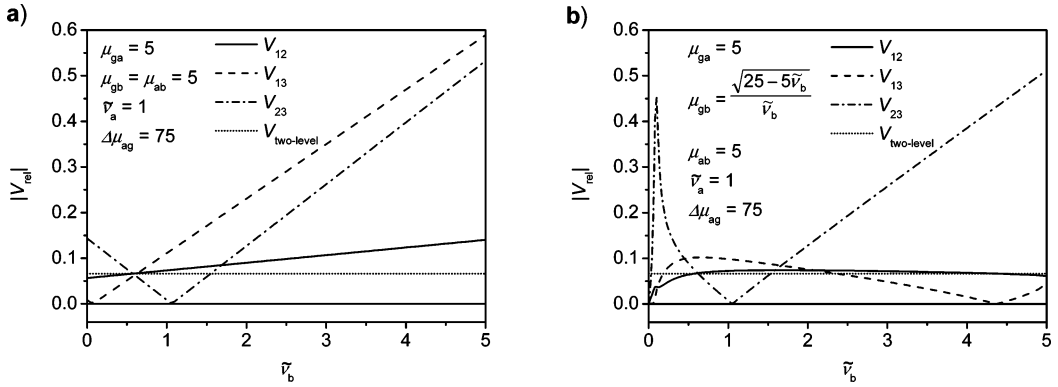

Figure 5. Plots of the absolute values of the electronic couplings derived by the GMH three-level model and GMH two-level model vs $\tilde{\nu}_b$. At positions with $|V_{rel}| = 0$, a change in sign of the relative electronic coupling V_{rel} occurs.

TABLE 3: Adiabatic (calculated and experimental)[63] and Diabatic Transition Moments Calculated by the GMH Three-level Model in D

		μ_{gg}	μ_{aa}	μ_{bb}	μ_{ga}	μ_{gb}	μ_{ab}	μ_{11}	μ_{22}	μ_{33}
	AM1-CISD[a]	−33.4	33.2	7.3	18.5	1.0	9.4	−38.2	40.6	4.7
1$^{\bullet+}$[b]	+ COSMO[a]	−34.1	30.8	7.7	2.3	2.1	7.7	−34.3	33.2	5.4
	exp.[a,c]				7.6	5.4		−35.5	34.3	5.6
	AM1-CISD[a]	−35.5	33.7	−14.3	22.2	6.3	12.7	−42.2	43.6	−17.4
4$^{\bullet+}$	+ COSMO[a]	−36.9	29.1	−6.1	6.5	8.9	7.1	−39.6	31.5	−5.8
	exp.[a,c]				3.4	5.9		−38.1	30.8	−6.6
	AM1-CISD[a]	−20.0	22.6	3.7	10.8	2.0	2.1	−22.7	25.5	3.5
5$^{\bullet+}$	+ COSMO[a]	−20.7	21.7	−0.6	0.5	2.5	0.9	−21.0	21.7	−0.3
	exp.[a,c]				2.6	3.2		−21.3	21.9	−0.2
	AM1-CISD[a]	−21.3	18.6	−5.8	5.6	1.0	4.3	−22.1	20.1	−6.5
6$^{\bullet+}$	+ COSMO[a]	−32.2	20.2	−2.9	4.7	1.3	3.4	−32.7	21.1	−3.4
	exp.[a,c]				7.5	5.4		−34.0	21.9	−2.8
	AM1-CISD[a]	−50.0	51.2	−8.2	27.3	8.2	9.7	−57.5	60.0	−9.5
9$^{\bullet+}$	+ COSMO[a]	−51.2	47.5	0.9	3.6	9.7	10.2	−53.0	49.9	0.2
	exp.[a,c]				0.9	5.2		−51.7	49.7	−0.8

[a] Odd number of positive off-diagonal transition moments. [b] Extinction coefficients were estimated under the assumption that the monoradical cation **1**$^{\bullet+}$ shows a $\pi-\pi^*$ band half as intense as the dication **1**$^{2+}$.[65] [c] For the three-level GMH analysis, the experimental values and, where lacking, the COSMO ($\epsilon = 2.0$) values were used.

TABLE 4: Transition Energies (computed and experimental) and Diabatic Electronic Couplings (GMH) in cm^{-1}

		$\tilde{\nu}_a$	$\tilde{\nu}_b$	V_{12}[a]	V_{13}[a]	V_{23}[a]	$V_{two-level}$[b]
	AM1-CISD[c]	10 730	16 120	2410	1180	1650	2600
1$^{\bullet+}$[e]	+ COSMO[d]	11 900	16 700	560	600	1320	420
	exp.[d,f]	6230	11 870	970	990	1550	710
	AM1-CISD[d]	8640	11 310	2380	480	540	2330
4$^{\bullet+}$	+ COSMO[d]	10 030	13 060	1320	2850	340	970
	exp.[d,f]	6600	10 710	570	1760	720	340
	AM1-CISD[d]	9850	16 330	2280	620	670	2230
5$^{\bullet+}$	+ COSMO[d]	10 370	16 390	180	1970	230	120
	exp.[d,f]	6280	10 620	430	1550	150	380
	AM1-CISD[d]	4160	9930	590	160	950	560
6$^{\bullet+}$	+ COSMO[d]	5620	11 380	530	310	810	500
	exp.[d,f]	7500	11 590	1220	1590	510	1030
	AM1-CISD[d]	9190	12 790	2280	1040	420	2180
9$^{\bullet+}$	+ COSMO[d]	10 790	14 570	730	2390	680	390
	exp.[d,f]	7500	11 100	220	1070	710	70

[a] Obtained by the GMH three-level model. [b] Obtained by the GMH two-level model (eq 1). [c] Even number of positive coupling values. [d] Odd number of positive coupling values. [e] Extinction coefficients were estimated using corrected spectra under the assumption that the monoradical cation **1**$^{\bullet+}$ shows a $\pi-\pi^*$ band half as intense as the dication **1**$^{2+}$.[65] [f] For the three-level GMH analysis, the experimental values and, where lacking, the COSMO (in the solvent) values were used.

TABLE 5: Dipole Moment Differences in D

	$\Delta\mu_{ag}$[a]	$\Delta\mu_{bg}$[a]	$\Delta\mu_{12}$[b]	$\Delta\mu_{13}$[b]
1$^{\bullet+}$	64.9	41.8	67.6	39.7
4$^{\bullet+}$	66.0	30.8	68.9	31.5
5$^{\bullet+}$	42.4	20.1	43.2	21.1
6$^{\bullet+}$	52.4	29.3	55.9	31.2
9$^{\bullet+}$	98.7	52.1	101.4	50.9

[a] Differences of the AM1-CISD + COSMO dipole moments. [b] Differences of the diabatic GMH transition moments derived from experimental input (see Table 3).

are different suggests that the Condon approximation (μ independent of the nuclear coordinates) is invalid. The computed transition energies $\tilde{\nu}_a$ and $\tilde{\nu}_b$ of the paracyclophane derivatives are all significantly larger than the experimental values while both computed energies $\tilde{\nu}_a$ and $\tilde{\nu}_b$ of the *p*-xylene derivative **6**$^{\bullet+}$ are somewhat smaller than the experimental values. In general, the inclusion of the COSMO solvent model does not improve the agreement.

The GMH analysis yields the electronic couplings V_{12}, V_{13}, and V_{23} given in Table 4. Those values that are derived only from computed energies and transition dipole moments show a distinct deviation from the couplings derived from the experimental in combination with computed values (= exp. in Tables 3 and 4). This is due to the fact that the computed transition energies are too large compared to the experimental values. In the discussion below, we therefore exclusively consider the values obtained from the combination of experimental and computed data.

The diabatic coupling V_{12} is a measure for the electronic interaction between the diabatic states (1) and (2) and characteristic for the intervalence charge transfer. The couplings V_{13} between the diabatic states (1) and (3) as well as V_{23} between states (2) and (3) are both attributed to triarylamine to bridge charge transfer. As expected, the smallest V_{12} was found for MV compound **9**$^{\bullet+}$ with the largest N−N distance.[29] For the two compounds with different connectivity, the pseudo-para isomer **4**$^{\bullet+}$ and the pseudo-ortho isomer **5**$^{\bullet+}$, we obtained a somewhat larger coupling for **4**$^{\bullet+}$ although the N−N distance is much larger in this case. However, for these two isomers, the number of bondings between the two redox centers is the same and the similar couplings for **4**$^{\bullet+}$ and **5**$^{\bullet+}$ prove that the coupling is provided by the bond pathway and not directly between the triarylamine moieties. The coupling V_{12} of the smallest cyclophane **1**$^{\bullet+}$ is, as expected, higher than those of **4**$^{\bullet+}$ and **5**$^{\bullet+}$ and smaller than V_{12} of **6**$^{\bullet+}$. For the π-conjugated *p*-xylene **6**$^{\bullet+}$, we obtain the largest V_{12}. Thus, direct conjugation obviously leads to stronger electronic interactions than the through-bond and through-space interactions provided by [2.2]-paracyclophane. Nevertheless, from the order of magnitude of

TABLE 6: AM1-CISD + COSMO Results of $4^{\bullet+}$ in Comparison to $4_{mod}^{\bullet+}$

	$4^{\bullet+}$	$4_{mod}^{\bullet+}$		$4^{\bullet+}$	$4_{mod}^{\bullet+}$
$\tilde{\nu}_a$/cm^{-1}	10 030	9540	μ_{bb}/D	−6.1	15.6
$\tilde{\nu}_b$/cm^{-1}	13 060	13 080	μ_{ga}/D	6.5	11.8
μ_{gg}/D	−36.9	−37.5	μ_{gb}/D	8.9	6.3
μ_{aa}/D	29.1	20.6			
μ_{ab}/D	7.1	11.0			

CHART 2

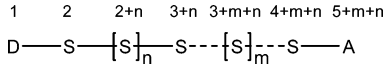

the couplings of the [2.2]paracyclophane derivatives, we assume that this bridge is able to mediate significant through-space and through-bond interactions. The through-space interaction of the [2.2]paracyclophane moiety occurs via direct overlap of the π-orbitals of the two unsaturated rings, and the through-bond interactions occur via the σ-orbitals of the two ethanediyl bridges. To separate these two interactions, we performed a calculation of $\mathbf{4}^{\bullet+}$ with the modification that the two ethanediyl bridges were replaced by four hydrogen atoms with a fixed carbon−hydrogen distance of 1.1 Å. All other atoms remained as in the optimized geometry of $\mathbf{4}^{\bullet+}$. The CISD results are given in Table 6 where $\mathbf{4}_{mod}^{\bullet+}$ is the modified cyclophane without the ethanediyl bridges.

The transition energies $\tilde{\nu}_a$ and $\tilde{\nu}_b$ and the dipole moment of the ground-state μ_{gg} do not vary greatly after removal of the ethanediyl bridges, but all transition moments and particularly the dipole moments μ_{aa} and μ_{bb} are affected by this modification. Hence, we infer that both the through-space as well as the through-bond interactions have a significant influence on the electronic properties of MV compounds and, thus, on the communication between the two redox centers.

The couplings $V_{two-level}$ derived from the GMH two-level model are somewhat smaller than the V_{12} values, but they show similar trends. Because the couplings V_{12} and $V_{two-level}$ depend on the N−N distance (see $\mathbf{9}^{\bullet+}$ vs $\mathbf{4}^{\bullet+}$), we conclude that the [2.2]paracyclophane moiety is not the limiting factor which governs the intramolecular charge transfer.

At this point, the question arises, what are the determining factors for the electronic couplings? To elucidate this aspect, we use McConnell's superexchange model in the formulation by Newton et al. (eq 10).[67,68] This model is valid in the perturbation limit with $|H/E| < 1$ where $H_{i,j}$ are the electronic coupling elements between states localized at adjacent centers and E is the respective energy relative to the ground state. Only nearest neighbor (NN) interactions are being considered. We stress that this approximation cannot be directly compared to our GMH three-level model presented above because the GMH model considers only those states which are experimentally accessible, that is, the states which are visible in the absorption spectra and where a dominating, direct donor−acceptor interaction is involved which invalidates the NN approximation.

We consider a general model system consisting of a donor D, an acceptor A, and a number of bridge sites S being connected by both $n + 1$ saturated spacers "−" (saturated bridge sites) and $m + 1$ unsaturated spacers "- -" (unsaturated bridge sites). Those sites being connected by saturated spacers (weak coupling) all have site energy E_1; those being connected by unsaturated spacers all shall have site energy E_2. The electronic coupling between the donor and first bridge site is $H_{1,2}$, that between the last bridge site and the acceptor is $H_{4+m+n,5+m+n}$. The electronic coupling between the equivalent bridge sites connected by saturated spacers is $H_{2,3}$ and that between

CHART 3

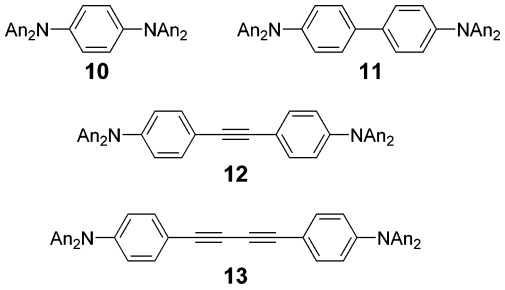

unsaturated spacers is $H_{3+n,4+n}$ (Chart 2). Then the effective electronic coupling V_{eff} follows from eq 10.

$$V_{eff} = \frac{H_{1,2}}{E_1} H_{4+m+n,5+m+n} \left(\frac{H_{2,3}}{E_1}\right)^{n+1} \left(\frac{H_{3+n,4+n}}{E_2}\right)^{m+1} \quad (10)$$

The $\ln(V_{eff})$ (eq 11) shows a linear relation with both the number $n + 1$ of sites connected by saturated spacers and/or with the number of unsaturated spacers $m + 1$.

$$\ln(V_{eff}) = \ln\left(\frac{H_{1,2}}{E_1}\right) + \ln(H_{4+m+n,5+m+n}) + (n+1)\ln\left(\frac{H_{2,3}}{E_1}\right) + (m+1)\ln\left(\frac{H_{3+n,4+n}}{E_2}\right) \quad (11)$$

Because $|H/E| < 1$, the third and fourth terms of eq 11 have a negative slope as expected for a superexchange model. From eq 11, it is obvious that because $H_{3+n,4+n}$ is much larger than $H_{2,3}$, varying the number $n + 1$ of saturated bridge sites yields a linear correlation with a steep but negative slope while varying the number $m + 1$ of unsaturated bridge sites yields a much smaller negative slope in agreement with enumerable experimental and theoretical findings.[69−73] For example, by varying unsaturated bridge sites, the onset of the correlation is $\ln(H_{1,2}/E_1) + \ln(H_{4+m+n,5+m+n}) + (n+1)\ln(H_{2,3}/E_1)$, that is, a higher number n of saturated bridge sites shifts the correlation vertically to smaller values of V_{eff}. By varying saturated bridge sites, the onset is $\ln(H_{1,2}/E_1) + \ln(H_{4+m+n,5+m+n}) + (m+1)\ln(H_{3+n,4+n}/E_2)$. Because $|(m+1)\ln(H_{3+n,4+n}/E_2)| < |(n+1)\ln(H_{2,3}/E_1)|$ for $m = n$, the onset shift is smaller for the correlation of varying saturated bridge sites than for varying unsaturated bridge sites.

Coming back to the real system $\mathbf{6}^{\bullet+}$ and, in addition, to the known systems $\mathbf{10}^{\bullet+}$−$\mathbf{13}^{\bullet+}$ [29] (see Chart 3), where only unsaturated bridges of different length (i.e., varying m values) separate the triarylamines, and the systems $\mathbf{1}^{\bullet+}$, $\mathbf{4}^{\bullet+}$, $\mathbf{5}^{\bullet+}$, and $\mathbf{9}^{\bullet+}$, where an additional unsaturated cyclophane is incorporated, one would expect from the above stated arguments that both series of systems exhibit linear correlations with the same negative slope but that the series $\mathbf{1}^{\bullet+}$, $\mathbf{4}^{\bullet+}$, $\mathbf{5}^{\bullet+}$, $\mathbf{9}^{\bullet+}$ has a smaller onset than the series $\mathbf{6}^{\bullet+}$, $\mathbf{10}^{\bullet+}$−$\mathbf{13}^{\bullet+}$.

In fact, a logarithmic plot of V vs the number of bonds n separating the N centers is linear for $\mathbf{1}^{\bullet+}$, $\mathbf{4}^{\bullet+}$, $\mathbf{5}^{\bullet+}$, and $\mathbf{9}^{\bullet+}$ (see Figure 6).

In Figure 6, the couplings V of π-conjugated MV compounds with smaller bridges $\mathbf{10}^{\bullet+}$−$\mathbf{13}^{\bullet+}$ (see Chart 3) are also presented. The electronic couplings V_{vc} of $\mathbf{10}^{\bullet+}$−$\mathbf{12}^{\bullet+}$ were obtained by band shape analysis. We recently described the analysis of MV species $\mathbf{10}^{\bullet+}$ [48] and $\mathbf{11}^{\bullet+}$.[47] Applying an analogous procedure to analyze the spectrum of tolane $\mathbf{12}^{\bullet+}$ [29] yields $V_{vc} = 2400$ cm^{-1}. The coupling $V_{two-level}$ of $\mathbf{13}^{\bullet+}$ was obtained using the Mulliken−Hush formalism (eq 1) with $\Delta\mu_{12}$ derived from

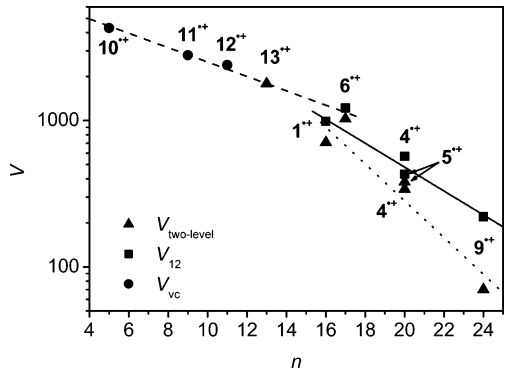

Figure 6. Logarithmic plot of electronic couplings V_{12}, $V_{\text{two-model}}$, and V_{vc} vs the number of bonds n separating the N centers and linear fits of the data as described in the text.

TD-DFT calculations.[39] As shown in Figure 6, the couplings of the π-conjugated MV systems **6**$^{\bullet+}$ (V_{12} and $V_{\text{two-level}}$) and **10**$^{\bullet+}$−**13**$^{\bullet+}$ also correlate linearly with n but the slope is somewhat smaller.

A simpler model that takes only one coupling value into account (eq 12) also reflects the exponential dependence of the coupling V on the distance r separating the redox centers. If we assume that the interactions occur through the bonds, then we can set the number of bonds n in relation with the distance r. In the following, we approximate that $r = 1.4\ \text{Å} \times n$.

$$V = V_0 e^{-(\beta r/2)}$$

or

$$\ln(V) = \ln(V_0) - \left(\frac{\beta r}{2}\right) \qquad (12)$$

The slope of the linear fits can, thus, be correlated to the β factor of eq 12. It was reported that this factor is ~1 Å^{-1} for saturated bridges[69,70,72] and significantly smaller (e.g., 0.46 Å^{-1})[73] for conjugated bridges.[71,73] We calculated the β values for the three linear fits in Figure 6. The conjugated MV systems **6**$^{\bullet+}$ (V_{12} and $V_{\text{two-level}}$) and **10**$^{\bullet+}$−**13**$^{\bullet+}$ show $\beta = 0.16$ Å^{-1} while the linear fit of V_{12} (**1**$^{\bullet+}$, **4**$^{\bullet+}$, **5**$^{\bullet+}$, and **9**$^{\bullet+}$) yields $\beta = 0.27$ Å^{-1} and the linear fit of $V_{\text{two-level}}$ (**1**$^{\bullet+}$, **4**$^{\bullet+}$, **5**$^{\bullet+}$, and **9**$^{\bullet+}$) results $\beta = 0.41$ Å^{-1}. Thus, the β values are all significantly smaller than 1 Å^{-1}, and β of the π-conjugated compounds is somewhat smaller than both β values of **1**$^{\bullet+}$, **4**$^{\bullet+}$, **5**$^{\bullet+}$, and **9**$^{\bullet+}$. As mentioned above from McConnell's superexchange model in the formulation by Newton et al., eq 10, we expect similar β values for both series **1**$^{\bullet+}$, **4**$^{\bullet+}$, **5**$^{\bullet+}$, **9**$^{\bullet+}$ and the π-conjugated species **6**$^{\bullet+}$ and **10**$^{\bullet+}$−**13**$^{\bullet+}$. This prediction is not fulfilled in our case, but the difference of the slope of **6**$^{\bullet+}$ and **10**$^{\bullet+}$−**13**$^{\bullet+}$ in comparison to the slopes of **1**$^{\bullet+}$, **4**$^{\bullet+}$, **5**$^{\bullet+}$, and **9**$^{\bullet+}$ (V_{12}) is small. Thus, the cyclophane bridge behaves more like an unsaturated spacer rather than a saturated bridge.

As the β value is small for the present type of π-conjugated MV compounds, we suppose that a larger number of bonds n and, therefore, longer π-conjugated bridges should still reveal a significant coupling in bis-triarylamine MV compounds. We therefore suppose that the bridge of a π-conjugated MV compound can, in principle, be significantly elongated and the MV compound will nevertheless have an analyzable IV-CT band.

TABLE 7: ET Parameters for All MV Compounds in CH_2Cl_2 Derived from GMH analysis and PES fits

	V_{IV}[a]/ cm^{-1}	V_{br}[a]/ cm^{-1}	λ_1[b]/ cm^{-1}	λ_2[b]/ cm^{-1}	C	$\Delta G°$ [b]/ cm^{-1}	ΔG^*[c]/ cm^{-1}
1$^{\bullet+}$	970	1270	6400	6000	−0.15	5400	1090
4$^{\bullet+}$	570	1240	7000	3200	0.16	6800	1180
5$^{\bullet+}$	430	850	6400	3300	0.13	7050	1110
6$^{\bullet+}$	1220	1050	8000	4500	0.10	6500	900
9$^{\bullet+}$	220	890	7700	3800	0.16	7000	1580

[a] ±50 cm^{-1}. [b] ±300 cm^{-1}. [c] ±100 cm^{-1}.

The two couplings V_{13} and V_{23} which affect the bridge state show significant differences, and this again reflects that the Condon approximation is not valid in these cases.

PES Parameter Fitting by Spectra Simulation. In the previous section, we demonstrated how to estimate electronic coupling values from linear optical characteristics of MV species. These evaluated GMH couplings can be used to calculate potential energy surfaces of the adiabatic states by solving the secular determinant (eq 13).

The construction of the adiabatic PES starts off with three diabatic (diagonal elements of eq 14) energy surfaces described by two-dimensional (2D) parabolic functions which were augmented by quartic terms (adjusted by parameter C). In this model, which we introduced in two recent papers,[34,44] we use two independent average modes x (asymmetric vibrational mode) and y (symmetric vibrational mode). The minima of the diabatic potential functions of states (1) and (2) each with the hole localized at one of the triarylamine redox centers (see Figure 1) are placed at $(x,y) = (0,0)$ and at $(x,y) = (1,0)$. The minimum of state (3) with the hole localized at the bridge is positioned at $(x,y) = (0.5,\sqrt{3}/2)$. Thus, the minima of the three diabatic states are located at the corners of an equilateral triangle with an edge length of unity. The bridge state (3) is shifted energetically by $\Delta G°$ relative to (1) while (2) and (1) are degenerate states. Two different Marcus reorganization energies are used within this model. One reorganization energy λ_1 is associated with (1) and (2), and a second reorganization energy λ_2 is associated with the bridge state (3). These two force constants are assumed to be equal for the x-mode and the y-mode. For the calculation of the adiabatic PES, we used the GMH derived coupling V_{12} for V_{IV} between states (1) and (2) as well as the averaged GMH couplings $V_{br} = (|V_{13}| + |V_{23}|)/2$ for the coupling between the triarylamine localized states and the bridge state (3). Thus, within this model we assume that the couplings are coordinate independent (Condon approximation).

The simulations of the IV-CT absorption and the bridge band were done in a classical manner with a Boltzmann distribution of the adiabatic ground state and vertical transitions to the IV-CT state and to the bridge state, respectively. The PESs were modeled by tuning the parameters λ_1, λ_2, $\Delta G°$, and C to give the best fit to the Gaussian bands (IV-CT and bridge) of the

$$\begin{vmatrix} \lambda_1\left[\frac{x^2 + Cx^4 + y^2 + Cy^4}{1+C}\right] - \epsilon & V_{IV} & V_{br} \\ V_{IV} & \lambda_1\left[\frac{(1-x)^2 + C(1-x)^4 + y^2 + Cy^4}{1+C}\right] - \epsilon & V_{br} \\ V_{br} & V_{br} & \lambda_2\left[\left(\frac{1}{2} - x\right)^2 + \left(\frac{\sqrt{3}}{2} - y\right)^2\right] + \Delta G° - \epsilon \end{vmatrix} = 0 \qquad (13)$$

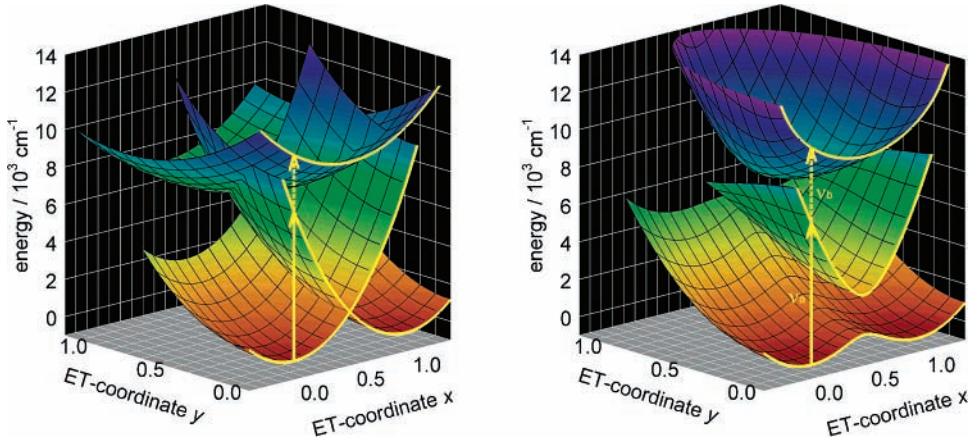

Figure 7. Diabatic (left) and adiabatic (right) potential energy surfaces of $\mathbf{6}^{\bullet+}$.

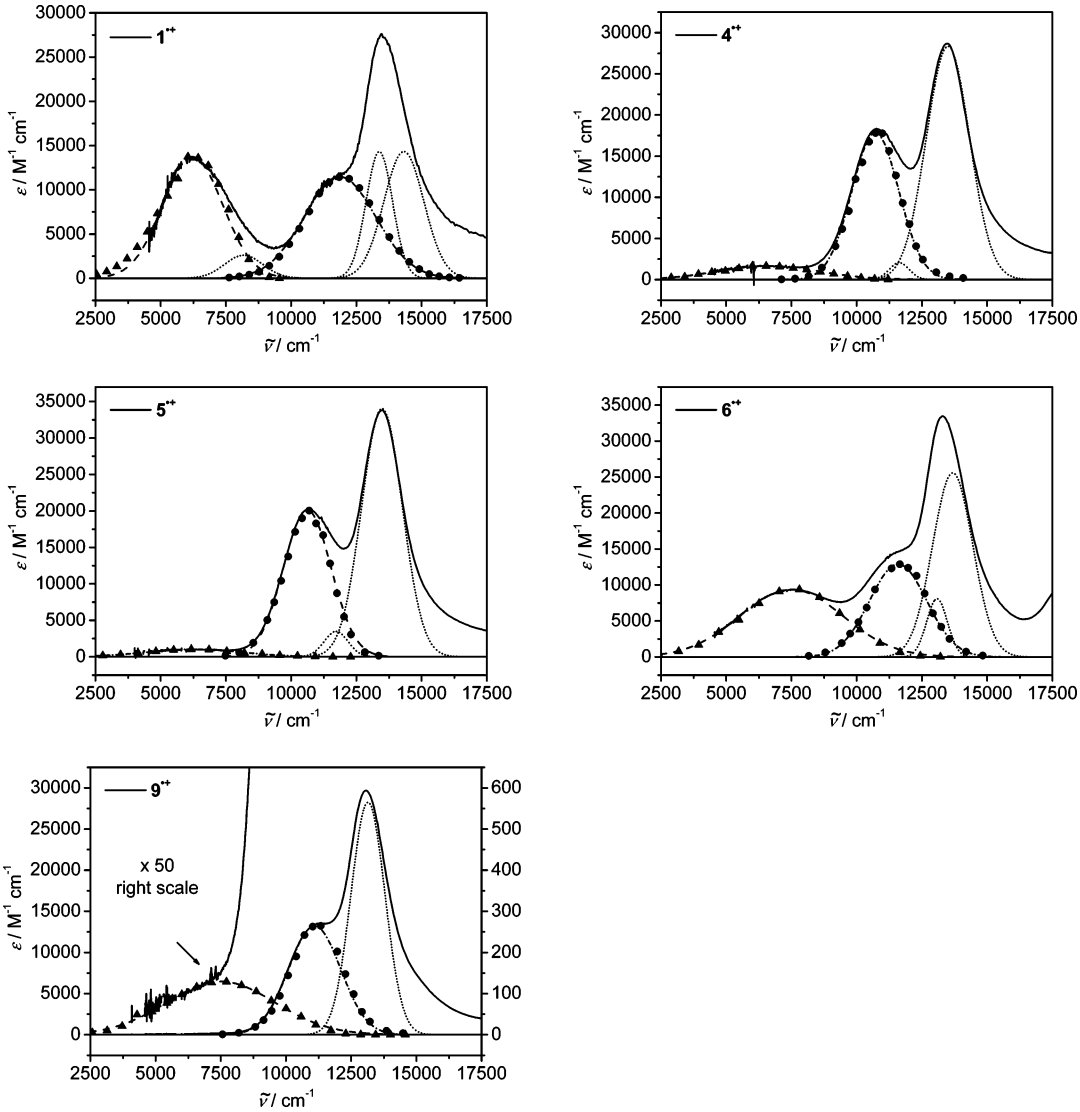

Figure 8. Absorption spectra of MV compounds $\mathbf{1}^{\bullet+}$, $\mathbf{4}^{\bullet+}$, $\mathbf{5}^{\bullet+}$, $\mathbf{6}^{\bullet+}$, and $\mathbf{9}^{\bullet+}$ in CH_2Cl_2 (solid), spectra deconvolution by Gaussian functions (IV-CT, dashed; bridge, dash−dotted; $\pi-\pi^*$, dotted), and PES spectra simulation (IV-CT, ▲; bridge, ●).

deconvoluted experimental absorption spectrum. As the parameters display no significant dependence on each other, only one parameter set is suitable for a stable fit and, therefore, the PES fitting procedure yields reliable values for λ_1, λ_2, and $\Delta G°$ (see Table 7).

The diabatic and the modeled adiabatic PES of $\mathbf{6}^{\bullet+}$ are presented in Figure 7. The yellow lines represent the 2D one-mode model which takes only the asymmetric electron-transfer coordinate x into account. The IV-CT and bridge absorption band simulated for the resulting PES are shown in Figure 8 where the experimental vis/NIR spectra in CH_2Cl_2 and the spectra deconvolution by Gaussian functions of $\mathbf{1}^{\bullet+}$, $\mathbf{4}^{\bullet+}$, $\mathbf{5}^{\bullet+}$, $\mathbf{6}^{\bullet+}$, and $\mathbf{9}^{\bullet+}$ are also presented. The negative parameter C of the PES fit of $\mathbf{1}^{\bullet+}$ is a consequence of the unexpectedly narrow

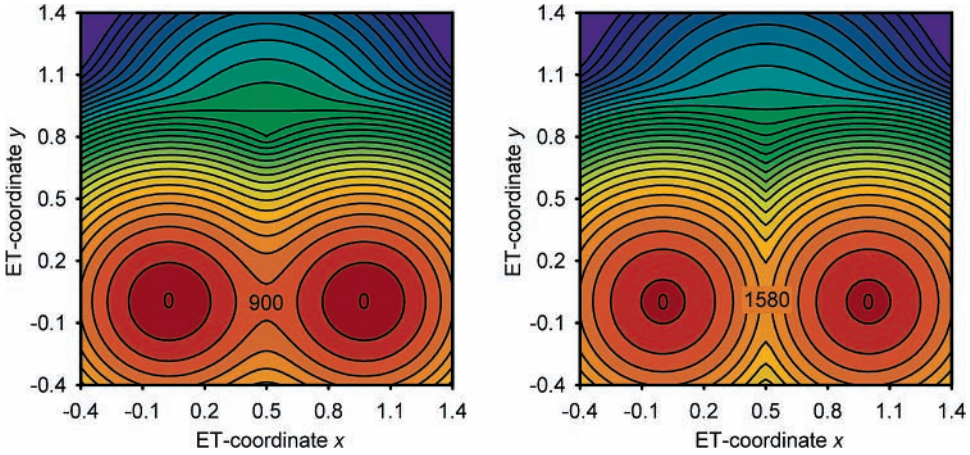

Figure 9. Contour plots of the adiabatic ground state PESs of $\mathbf{6}^{\bullet+}$ (left) and $\mathbf{9}^{\bullet+}$ (right), 350 cm^{-1} contour spacing.

IV-CT band (see above). The remaining PES fits yield positive values for parameter C as a result of broad IV-CT bands.

In general, the reorganization energy λ_1 varies little within the set of MV compounds ($\lambda_1 = 6300-8000$ cm^{-1}). The MV compounds $\mathbf{4}^{\bullet+}$, $\mathbf{5}^{\bullet+}$, $\mathbf{6}^{\bullet+}$, and $\mathbf{9}^{\bullet+}$ show small λ_2 values between 3200 and 4500 cm^{-1} while $\mathbf{1}^{\bullet+}$ has a significant larger value, $\lambda_2 = 6000$ cm^{-1}. The higher value for $\mathbf{1}^{\bullet+}$ might be due to the twisted biaryl moiety (AM1 computed twist angle: 58° in $\mathbf{1}^{\bullet+}$ compared to 46° in $\mathbf{3}^{\bullet+}$). The relative free energy $\Delta G°$ is very similar for all MV compounds (6500−7050 cm^{-1}) except for $\mathbf{1}^{\bullet+}$ and where the PES fitting procedure yields a somewhat smaller value (5400 cm^{-1}).

Contour plots of the adiabatic ground-state PESs of $\mathbf{6}^{\bullet+}$ and $\mathbf{9}^{\bullet+}$ are depicted in Figure 9. These PESs are representative for all MV species investigated in this study, and they all exhibit a double minimum. All adiabatic ground-state PESs show a weak impression at the position of the diabatic bridge state potential but without provoking an additional minimum. In a recent study, we showed that a third minimum in the PES is obtained for a more electron-rich *p*-dimethoxybenzene bridge and, thus, in such a system electron hopping and superexchange may be two coexisting thermal ET mechanisms.[34,44] In our case, depending on the free enthalpy difference $\Delta G°$, the bay is more or less profound. A small $\Delta G°$ value results in a deeper impression while larger $\Delta G°$ values cause a less pronounced smooth bay in the adiabatic ground-state PES. Nevertheless, these findings preclude a hopping mechanism for the thermal ET and, therefore, ET can occur solely by a superexchange mechanism.

Because all the λ_1 values are very similar for the MV compounds, the adiabatic ET barrier ΔG^* between the two minima of the adiabatic PES decreases with increasing coupling V_{IV}. Consequently, ΔG^* is relatively small for the π-conjugated MV compound $\mathbf{6}^{\bullet+}$ (900 cm^{-1}) and largest for $\mathbf{9}^{\bullet+}$ (1580 cm^{-1}).

Conclusions

The bis-triarylamines **1**, **4**−**6**, and **9** were synthesized by palladium and copper catalyzed C−C cross-coupling reactions (see Supporting Information). The vis/NIR spectra of the MV radical cations $\mathbf{1}^{\bullet+}$, $\mathbf{4}^{\bullet+}$−$\mathbf{6}^{\bullet+}$, and $\mathbf{9}^{\bullet+}$ were analyzed by a GMH model developed by Newton and Cave.[54] We used a GMH three-level model which takes into account two transitions: the intervalence charge transfer (IV-CT) transition and the bridge band which is associated with a triarylamine radical cation to bridge hole transfer. The model was applied to the MV species using both experimental transition energies and transition moments as well as AM1-CISD computed values in order to calculate the diabatic electronic coupling matrix elements. The diabatic coupling V_{12} is a measure for the electronic interaction between the triarylamine localized diabatic states (1) and (2) and is, therefore, characteristic for the intervalence charge transfer. This coupling V_{12} increases from $\mathbf{9}^{\bullet+}$ over the cyclophanes $\mathbf{5}^{\bullet+}$, $\mathbf{4}^{\bullet+}$, and $\mathbf{1}^{\bullet+}$ to the π-conjugated *p*-xylene $\mathbf{6}^{\bullet+}$. Thus, within this set of [2.2]paracyclophanes, the coupling increases with an increasing number of bonds. The similar couplings of the two isomers $\mathbf{5}^{\bullet+}$ and $\mathbf{4}^{\bullet+}$ which have the same numbers of bonds between the redox centers but different N−N distances prove that the hole transfer is always provided by the bond pathway and not directly between the two triarylamine moieties. The direct π-conjugation of $\mathbf{6}^{\bullet+}$ leads to a stronger electronic coupling $V_{12} = 1220$ cm^{-1} than the through-bond and through-space interactions provided by the [2.2]paracyclophane bridge. Nevertheless, we assume that the [2.2]paracyclophane bridge is able to mediate significant through-space and through-bond interactions because the [2.2]paracyclophane derivatives show still significant couplings V_{12} between 220 and 970 cm^{-1}. The electronic couplings $V_{two-level}$ derived from the GMH two-level model (eq 1) are somewhat smaller than V_{12}, but they show similar trends.

AM1-CISD calculations on the MV species $\mathbf{4}_{mod}^{\bullet+}$ which is similar to $\mathbf{4}^{\bullet+}$ but with the ethanediyl bridges of the [2.2]-paracyclophane moiety being replaced by hydrogen atoms reveal that both the through-space interaction which occurs via direct overlap of the π-orbitals of the two unsaturated rings of the cyclophane and the through-bond interactions which occur via the σ-orbitals of the two ethanediyl bridges have significant influence on the communication between the two triarylamine units of the cyclophane bridged MV species.

McConnell's superexchange model predicts a linear correlation of ln(V) to the number of bridge sites with similar slopes for both series the cyclophanes $\mathbf{1}^{\bullet+}$, $\mathbf{4}^{\bullet+}$, $\mathbf{5}^{\bullet+}$, and $\mathbf{9}^{\bullet+}$ and the π-conjugated species as $\mathbf{6}^{\bullet+}$ and $\mathbf{10}^{\bullet+}$−$\mathbf{13}^{\bullet+}$. However, we found that the slope of the latter series is only slightly steeper than that of the conjugated series. Therefore, we conclude that the cyclophane bridge acts more like an unsaturated bridge than like a saturated spacer. These findings will have implications for the design of molecular materials based on cyclophane bridges.

The couplings derived from the GMH three-level model were used to calculate the PESs of the adiabatic states of $\mathbf{1}^{\bullet+}$, $\mathbf{4}^{\bullet+}$−$\mathbf{6}^{\bullet+}$, and $\mathbf{9}^{\bullet+}$. The ground-state PESs of $\mathbf{1}^{\bullet+}$, $\mathbf{4}^{\bullet+}$−$\mathbf{6}^{\bullet+}$, and $\mathbf{9}^{\bullet+}$ all show a double minimum which is typical for localized MV compounds. This finding confirms that HT solely occurs by a

superexchange mechanism in these cases and a hopping mechanism for the thermal HT can be precluded.

Cyclic Voltammetry. The electrochemical experiments were performed in superdry, argon-saturated CH_2Cl_2 with 0.15 M tetrabutylammonium hexafluorophosphate (TBAH) as the supporting electrolyte and ca. 0.002 M substrate using a conventional three-electrode setup with platinum disk electrode (0.12 cm^2). The potentials are referenced against ferrocene (Fc/Fc^+). The long-term reversibility of the processes was checked by performing multicycle thin-layer measurements at a 10 mV s^{-1} scan rate.

UV−Vis/NIR Spectroscopy. The UV−vis/NIR spectra of the radical cations and dications in MeCN were obtained by the stepwise addition of 10^{-2}−10^{-3} M $NOBF_4$/MeCN via a microliter syringe to a solution of the compounds ((3−7) × 10^{-5} M). Because the electron transfer (ET) is rather slow using $NOBF_4$ in MeCN one has to wait approximately 30 min after each addition before the spectrum could be recorded. The extinction coefficients obtained in MeCN are too small due to the slight instability of the radical cations under the conditions employed. The spectra in CH_2Cl_2 were obtained by the dropwise addition of 10^{-2}−10^{-3} M $SbCl_5/CH_2Cl_2$ in the same way. The quick oxidation process in CH_2Cl_2 allows very short periods between the addition of the oxidation agent and spectrum measurement. The extinction coefficients of the MV species in CH_2Cl_2 were obtained as already described in ref. 29, except the extinction coefficients of $\mathbf{1}^{\bullet+}$ which were estimated using corrected spectra under the assumption that the monoradical cation $\mathbf{1}^{\bullet+}$ shows a $\pi-\pi^*$ band half as intense as the dication $\mathbf{1}^{2+}$.[65] For the analysis of the absorption bands of the MV compounds, deconvolution of these spectra by four (five for $\mathbf{1}^{\bullet+}$) Gaussian functions were performed as described in the text above.

Semiempirical Calculations. All calculation were done using the AM1 parametrization implemented in the MOPAC97 program.[74] All optimizations were performed without symmetry restrictions in Cartesian coordinates by the eigenvector following (EF) routine. The configuration interaction included singles and doubles excitations (CISDs) within an active orbital window consisting of the four highest doubly occupied, one singly occupied, and the two lowest unoccupied orbitals. Pulay's procedure was used as the self-consistent field (SCF) converger of all calculations. The effect of the solvent (CH_2Cl_2) was simulated using COSMO including the parameters $\epsilon = 2.0$ and a radius of the solvent of 2.5 Å at the CISD optimized gas-phase structures. The experimental permittivity of CH_2Cl_2 is 8.9, but a previous study revealed that a smaller empirical permittivity yields more reliable results. The use of the experimental permittivity for the COSMO method results in an overestimation of the solvent influence on the CT absorption energies.[44]

Acknowledgment. We thank the Deutsche Forschungsgemeinschaft and the Volkswagenstiftung for financial support and the Wacker-Chemie GmbH as well as the Hereaus GmbH for the chemicals.

Supporting Information Available: Information describing the synthesis and experimental details of compounds **1**−**9** along with a schematic representation of the compounds. This material is available free of charge via the Internet at http://pubs.acs.org.

References and Notes

(1) Bazan, G. C.; Oldham, J., Jr.; Lachicotte, R. J.; Tretiak, S.; Chernyak, V.; Mukamel, S. *J. Am. Chem. Soc.* **1998**, *120*, 9188−9204.

(2) Verdal, N.; Godbout, J. T.; Perkins, T. L.; Bartholomew, G. P.; Bazan, G. C.; Kelley, A. M. *Chem. Phys. Lett.* **2000**, *320*, 95−103.

(3) Zyss, J.; Ledoux, I.; Volkov, S.; Chernyak, V.; Mukamel, S.; Bartholomew, G. P.; Bazan, G. C. *J. Am. Chem. Soc.* **2000**, *122*, 11956−11962.

(4) Bartholomew, G. P.; Bazan, G. C. *Acc. Chem. Res.* **2001**, *34*, 30−39.

(5) Bartholomew, G. P.; Bazan, G. C. *J. Am. Chem. Soc.* **2002**, *124*, 5183−5196.

(6) Moran, A. M.; Bartholomew, G. P.; Bazan, G. C.; Kelley, A. M. *J. Phys. Chem. A* **2002**, *106*, 4928−4937.

(7) Utz, N.; Koslowski, T. *Chem. Phys.* **2002**, *282*, 389−397.

(8) Bartholomew, G. P.; Rumi, M.; Pond, S. J. K.; Perry, J. W.; Tretiak, S.; Bazan, G. C. *J. Am. Chem. Soc.* **2004**, *126*, 11529−11542.

(9) Hong, J. W.; Woo, H. Y.; Liu, B.; Bazan, G. C. *J. Am. Chem. Soc.* **2005**, *127*, 7435−7443.

(10) Woo, H. Y.; Hong, J. W.; Liu, B.; Mikhailovsky, A.; Korystov, D.; Bazan, G. C. *J. Am. Chem. Soc.* **2005**, *127*, 820−821.

(11) Heilbronner, E.; Maier, J. P. *Helv. Chim. Acta* **1974**, *57*, 151−159.

(12) Sato, T.; Torizuka, K. *J. Chem. Soc., Perkin Trans. 2* **1978**, 1199−1204.

(13) Gerson, F.; Martin, W. B., Jr. *J. Am. Chem. Soc.* **1969**, *91*, 1883−1891.

(14) Gerson, F.; Martin, W. B.; Wydler, C. *J. Am. Chem. Soc.* **1976**, *98*, 1318−1320.

(15) Gerson, F.; Lopez, J.; Boekelheide, V.; Hopf, H. *Helv. Chim. Acta* **1982**, *65*, 1391−1397.

(16) Bruhin, J.; Gerson, F.; Ohyanishiguchi, H. *J. Chem. Soc., Perkin Trans. 2* **1980**, 1045−1050.

(17) Badger, B.; Brocklehurst, B. *Trans. Faraday Soc.* **1969**, *65*, 2582−2587.

(18) Kovac, B.; Mohraz, M.; Heilbronner, E.; Boekelheide, V.; Hopf, H. *J. Am. Chem. Soc.* **1980**, *102*, 4314−4324.

(19) Gerson, F.; Lopez, J.; Hopf, H. *Helv. Chim. Acta* **1982**, *65*, 1398−1403.

(20) Ohyanishiguchi, H.; Terahara, A.; Hirota, N.; Sakata, Y.; Misumi, S. *Bull. Chem. Soc. Jpn.* **1982**, *55*, 1782−1789.

(21) Wartini, A. R.; Valenzuela, J.; Staab, H. A.; Neugebauer, F. A. *Eur. J. Org. Chem.* **1998**, *139*, 9−148.

(22) Wartini, A. R.; Staab, H. A.; Neugebauer, F. A. *Eur. J. Org. Chem.* **1998**, *1161*, 1−1170.

(23) Nelsen, S. F.; Konradsson, A. E.; Telo, J. P. *J. Am. Chem. Soc.* **2005**, *127*, 920−925.

(24) Bonvoisin, J.; Launay, J.-P.; Van der Auweraer, M.; De Schryver, F. C. *J. Phys. Chem.* **1994**, *98*, 5052−5057; Erratum: **1996**, *100* (45), 18006.

(25) Bonvoisin, J.; Launay, J.-P.; Verbouwe, W.; Van der Auweraer, M.; De Schryver, F. C. *J. Phys. Chem.* **1996**, *100*, 17079−17082.

(26) Stickley, K. R.; Blackstock, S. C. *Tetrahedron Lett.* **1995**, *36*, 1585−1588.

(27) Lambert, C.; Nöll, G. *Angew. Chem., Int. Ed. Engl.* **1998**, *37*, 2107−2110.

(28) Lambert, C.; Nöll, G.; Schmalzlin, E.; Meerholz, K.; Bräuchle, C. *Chem.−Eur. J.* **1998**, *4*, 2129−2135.

(29) Lambert, C.; Nöll, G. *J. Am. Chem. Soc.* **1999**, *121*, 8434−8442.

(30) Lambert, C.; Nöll, G.; Hampel, F. *J. Phys. Chem. A* **2001**, *105*, 7751−7758.

(31) Coropceanu, V.; Malagoli, M.; Andre, J. M.; Brédas, J.-L. *J. Chem. Phys.* **2001**, *115*, 10409−10416.

(32) Lambert, C.; Nöll, G. *Chem.−Eur. J.* **2002**, *8*, 3467−3477.

(33) Coropceanu, V.; Malagoli, M.; Andre, J. M.; Brédas, J.-L. *J. Am. Chem. Soc.* **2002**, *124*, 10519−10530.

(34) Lambert, C.; Nöll, G.; Schelter, J. *Nat. Mater.* **2002**, *1*, 69−73.

(35) Lambert, C.; Nöll, G. *J. Chem. Soc., Perkin Trans. 2* **2002**, 2039−2043.

(36) Nelsen, S. F.; Konradsson, A. E.; Weaver, M. N.; Telo, J. P. *J. Am. Chem. Soc.* **2003**, *125*, 12493−12501.

(37) Lambert, C.; Nöll, G.; Zabel, M.; Hampel, F.; Schmalzlin, E.; Bräuchle, C.; Meerholz, K. *Chem.−Eur. J.* **2003**, *9*, 4232−4239.

(38) Lambert, C. *ChemPhysChem* **2003**, *4*, 877−880.

(39) Coropceanu, V.; Lambert, C.; Nöll, G.; Brédas, J.-L. *Chem. Phys. Lett.* **2003**, *373*, 153−160.

(40) Yano, M.; Ishida, Y.; Aoyama, K.; Tatsumi, M.; Sato, K.; Shiomi, D.; Ichimura, A.; Takui, T. *Synth. Met.* **2003**, *137*, 1275−1276.

(41) Yano, M.; Aoyama, K.; Ishida, Y.; Tatsumi, M.; Sato, K.; Shiomi, D.; Takui, T. *Polyhedron* **2003**, *22*, 2003−2008.

(42) Jones, S. C.; Coropceanu, V.; Barlow, S.; Kinnibrugh, T.; Timofeeva, T.; Brédas, J. L.; Marder, S. R. *J. Am. Chem. Soc.* **2004**, *126*, 11782−11783.

(43) Coropceanu, V.; Gruhn, N. E.; Barlow, S.; Lambert, C.; Durivage, J. C.; Bill, T. G.; Nöll, G.; Marder, S. R.; Brédas, J.-L. *J. Am. Chem. Soc.* **2004**, *126*, 2727−2731.

(44) Lambert, C.; Amthor, S.; Schelter, J. *J. Phys. Chem. A* **2004**, *108*, 6474−6486.
(45) Szeghalmi, A. V.; Erdmann, M.; Engel, V.; Schmitt, M.; Amthor, S.; Kriegisch, V.; Nöll, G.; Stahl, R.; Lambert, C.; Leusser, D.; Stalke, D.; Zabel, M.; Popp, J. *J. Am. Chem. Soc.* **2004**, *126*, 7834−7845.
(46) Heckmann, A.; Lambert, C.; Goebel, M.; Wortmann, R. *Angew. Chem., Int. Ed.* **2004**, *43*, 5851−5856.
(47) Low, P. J.; Paterson, M. A. J.; Puschmann, H.; Goeta, A. E.; Howard, J. A. K.; Lambert, C.; Cherryman, J. C.; Tackley, D. R.; Leeming, S.; Brown, B. *Chem.−Eur. J.* **2004**, *10*, 83−91.
(48) Lambert, C.; Risko, C.; Coropceanu, V.; Schelter, J.; Amthor, S.; Gruhn, N. E.; Durivage, J.; Brédas, J.-L. *J. Am. Chem. Soc.* **2005**, *127*, 8508−8516.
(49) Barlow, S.; Risko, C.; Coropceanu, V.; Tucker, N. M.; Jones, S. C.; Levi, Z.; Khrustalev, V. N.; Antipin, M. Y.; Kinnibrugh, T. L.; Timofeeva, T.; Marder, S. R.; Brédas, J. L. *Chem. Commun.* **2005**, 764−766.
(50) Chiu, K. Y.; Su, T. H.; Huang, C. W.; Liou, G. S.; Cheng, S. H. *J. Electroanal. Chem.* **2005**, *578*, 283−287.
(51) Dümmler, S.; Roth, W.; Fischer, I.; Heckmann, A.; Lambert, C. *Chem. Phys. Lett.* **2005**, *408*, 264−268.
(52) Lambert, C.; Schelter, J.; Fiebig, T.; Mank, D.; Trifonov, A. *J. Am. Chem. Soc.* **2005**, *127*, 10600−10610.
(53) Creutz, C.; Newton, M. D.; Sutin, N. J. *J. Photochem. Photobiol., A* **1994**, *82*, 47−59.
(54) Cave, R. J.; Newton, M. D. *Chem. Phys. Lett.* **1996**, *249*, 15−19.
(55) Newton, M. D. *Adv. Chem. Phys.* **1999**, *106*, 303−375.
(56) Cave, R. J.; Newton, M. D.; Kumar, K.; Zimmt, M. B. *J. Phys. Chem.* **1995**, *99*, 17501−17504.
(57) Cave, R. J.; Newton, M. D. *J. Chem. Phys.* **1997**, *106*, 9213−9226.
(58) Nelsen, S. F.; Newton, M. D. *J. Phys. Chem. A* **2000**, *104*, 10023−10031.
(59) Newton, M. D. *Theor. Chem. Acc.* **2003**, *110*, 307−321.
(60) Shin, Y. G. K.; Newton, M. D.; Isied, S. S. *J. Am. Chem. Soc.* **2003**, *125*, 3722−3732.
(61) Lappe, J.; Cave, R. J.; Newton, M. D.; Rostov, I. V. *J. Phys. Chem. B* **2005**, *109*, 6610−6619.
(62) Nadeau, J. M.; Liu, M.; Waldeck, D. H.; Zimmt, M. B. *J. Am. Chem. Soc.* **2003**, *125*, 15964−15973.
(63) The GMH theory uses the projection of the transition dipole moment vectors in one defined direction. In this paper, we use the projections of all vectors on the N−N axis of each molecule. For the dipole moment of ions, we used the center of mass as the origin.
(64) Amthor, S.; Noller, B.; Lambert, C. *Chem. Phys.* **2005**, *316*, 141−152.
(65) To calculate the extinction coefficients of the radical cation spectrum, it is necessary to estimate the comproportionation constant K_{co}. In general, K_{co} is calculated by $K_{co} = 10^{(\Delta E/0.059)}$ using the redox potential splittings ΔE obtained by fitting the cyclic voltammogram. Calculation of the extinction coefficient following this procedure yields an unexpectedly weak $\pi-\pi^*$ band of $\mathbf{1}^{\bullet+}$. This may be a consequence of an error in ΔE which leads to the wrong extinction coefficients of the absorption spectrum. We can definitely rule out decomposition processes or kinetically hindered, and thus slow, oxidation processes because the dication $\mathbf{1}^{2+}$ shows a $\pi-\pi^*$ band twice as intense as the monoradical cation $\mathbf{2}^{\bullet+}$ and $\mathbf{3}^{\bullet+}$ and similar to those of $\mathbf{4}^{2+}$, $\mathbf{5}^{2+}$, $\mathbf{6}^{2+}$, and $\mathbf{9}^{2+}$.[75] We therefore calculated the extinction coefficients of $\mathbf{1}^{\bullet+}$ under the assumption that the monoradical cation $\mathbf{1}^{\bullet+}$ shows a $\pi-\pi^*$ band half as intense as the dication $\mathbf{1}^{2+}$. From the resulting extinction coefficients, we infer that the corresponding comproportionation constant $K_{co} = 2.8 \times 10^{-3}$ and $\Delta E = -91$ mV. Negative ΔE values were determined, for example, for 2,5-disubstituted furans[76] and are due to a second redox process which is at a more negative potential than the first, that is, if the second oxidation is facilitated and the dication is particularly stabilized. The CV signal of $\mathbf{1}^{\bullet+}$ has a peak width at half-height = 70 mV.; however, for negative ΔE values, a peak width at half-height <57 mV is expected.[76] Nevertheless, the experimental CV could be broadened by a remaining uncompensated resistance particularly in the low-polarity CH_2Cl_2.
(66) Zhu, Y.; Wolf, M. O. *J. Am. Chem. Soc.* **2000**, *122*, 10121−10125.
(67) Newton, M. D. *Chem. Rev.* **1991**, *91*, 767−792.
(68) Newton, M. D.; Cave, R. J. In *Molecular Electronics*; Jortner, J., Ratner, M., Eds.; Blackwell: Malden, MA, 1997.
(69) Closs, G. L.; Calcaterra, L. T.; Green, N. J.; Penfield, K. W.; Miller, J. R. *J. Phys. Chem.* **1986**, *90*, 3673−3683.
(70) Johnson, M. D.; Miller, J. R.; Green, N. S.; Closs, G. L. *J. Phys. Chem.* **1989**, *93*, 1173−1176.
(71) Creager, S.; Yu, C. J.; Bamdad, C.; O'Connor, S.; MacLean, T.; Lam, E.; Chong, Y.; Olsen, G. T.; Luo, J. Y.; Gozin, M.; Kayyem, J. F. *J. Am. Chem. Soc.* **1999**, *121*, 1059−1064.
(72) Smalley, J. F.; Finklea, H. O.; Chidsey, C. E. D.; Linford, M. R.; Creager, S. E.; Ferraris, J. P.; Chalfant, K.; Zawodzinsk, T.; Feldberg, S. W.; Newton, M. D. *J. Am. Chem. Soc.* **2003**, *125*, 2004−2013.
(73) Weiss, E. A.; Ahrens, M. J.; Sinks, L. E.; Gusev, A. V.; Ratner, M. A.; Wasielewski, M. R. *J. Am. Chem. Soc.* **2004**, *126*, 5577−5584.
(74) Stewart, J. J. P. *MOPAC97*; Fujitsu Limited: Tokyo, Japan, 1997.
(75) Amthor, S.; Lambert, C. Dications of Bis-triarylamino-[2.2]-paracyclophanes: Evaluation of Excited-State Couplings by GMH Analysis. *J. Phys. Chem. A*, submitted for publication, 2005.
(76) Salbeck, J.; Schoberl, U.; Rapp, K. M.; Daub, J. *Z. Phys. Chem.* **1991**, *171*, 191−212.